Understanding the Variability in GeAsTe Ovonic Threshold Switching Devices

Z. Hu †(1), G. Wang †(1), Z. Chai(2), W. Zhang*(1)(*w.zhang@ljmu.ac.uk), D. Garbin(3), R. Degraeve (3), S. Clima(3), T. Ravsher(3), A. Fantini(3), J. F. Zhang(1), A. Belmonte(3), G. S. Kar(3)

(1)School of Engineering, Liverpool John Moores University, Liverpool L3 3AF, UK, †equal contributions,

(2)Xi'an Jiaotong University, China, (3)IMEC, Leuven B3001, Belgium

Abstract -- Ovonic threshold switching (OTS) devices have recently demonstrated strong performance as selectors in high-density cross-point 1S1R emerging memory arrays to suppress the sneak current path and as selector-only-memory (SOM), with excellent I_{on}, I_{on}/I_{off} nonlinearity, and endurance. However, a detailed variability study is still lacking, and understanding of the responsible mechanisms is limited. In this work, different cycle-to-cycle (C2C) V_{th} variability mechanisms in GeAsTe OTS are identified: (i) Defects that remain active at the off-state lead to the less than 0.2 V intrinsic small random variability (SRV); (ii) Defects activated at the on-state result in up to 1 V large pseudo-random variability (LPV). Novel techniques such as the fast frequency-domain noise analysis and the sequential variability analysis are developed to identify the SRV and LPV mechanisms and to characterize their statistical correlations with different defects. The observed single modal, bimodal and multimodal C2C V_{th} variability distributions can be explained by the combination of SRV and LPV at different pulse operation conditions. This work provides critical guidance for OTS variability optimization.

I. Introduction

Ovonic threshold switching (OTS) devices have been reported recently with high I_{on}, low I_{off}, excellent thermal stability and endurance [1-3]. We have also reported on its switching and reliability mechanisms both as the selector and selector-only memory devices [4-11]. Reducing the V_{th} variability in selector devices is one of the key requirements in high-density cross-point emerging memory arrays [1,7-10]. A detailed study on its variability mechanisms is still lacking, and the understanding is limited, such as on the complex multimodal V_{th} distributions (**Figs.1a-c**) [7-9]. **In this work**, a comprehensive analysis of C2C variability mechanisms and the associated defects in GeAsTe OTS finds, for the first time, that defects remaining active in the off-state contribute to intrinsic small random variability (SRV), while defects activated during the on-state period lead to large pseudo-random variability (LPV) that includes a significant V_{th} jump followed by gradual recovery. To investigate these phenomena, novel techniques such as the fast frequency-domain noise analysis and the sequential variability analysis are developed to identify the SRV and LPV mechanisms and their statistical correlations with different defects. Different V_{th} CDF distributions that exhibit single-, bi-, and multimodal behaviors can be explained by the combination of SRV and LPV under various practical pulse operational conditions, providing valuable insights for optimizing OTS variability.

II. Device and different variability

Devices used: Amorphous GeAsTe films are prepared by room temperature physical vapor deposition (PVD) (**Fig.2a**) [4-7]. TiN/GeAsTe/TiN device is integrated in a 300 mm process flow, using a pillar (TiN) bottom electrode that defines the device size from 135 nm down to 50 nm. A GeAsTe chalcogenide film with 20 nm thickness was deposited and passivated with a low-temperature BEOL process. A triangular or rectangular pulse is used to record the I-V during pulse edge to extract V_{th} for 1S1R and OTS-only [10] (**Fig.2b**). Novel techniques for characterizing different types of variability will be introduced in each corresponding section.

Typical Variability: A typical variability result of V_{th}, measured in 150 cycles, is shown in **Fig.3a**, with its CDF distribution in **Fig.3b**. Instead of exhibiting unimodal randomness, the cycle-to-cycle V_{th} variations reveal several discernible patterns. In most cycles, V_{th} shows small random variability. In certain cycles, large pseudo random variability is observed, which consists of a large V_{th} jump followed by a gradual V_{th} recovery process. The large V_{th} jump and recovery leads to a bimodal V_{th} distribution that has been observed in many previous reports [7-9,14], but there is a lack of convincing explanations. In this work, an in-depth investigation on the different types of variability will start with the SRV, which does not have the most significant impact in OTS. Its mechanism is correlated to the intrinsic defects at the off-state and will set the benchmark for characterizing the LPV in Section IV.

III. SRV characterization and mechanism

SRV is independent of operation conditions. A typical SRV result is shown in **Fig.4a&b**, where V_{th} shows a single-modal Gaussian distribution with small total variations less than 0.2 V. The impact of series resistances R_s are compared in **Fig. 4b**, where the OTS-only V_{th} increases with R_s. However, V_{th} variation remains almost the same. The larger V_{th} suggests that weaker defect clusters are formed for switching at larger R_s [8,10]. SRV, on the other hand, is independent of the defect cluster diameters, indicating that the defects responsible for the intrinsic OTS switching are distributed uniformly, so that different cluster diameters do not lead to further variations. This can be further supported by comparing different OTS devices with the same R_s value but different first firing voltages, V_{FF}. As shown in **Fig.4c**, a larger V_{FF} leads to stronger defect clusters hence a smaller V_{th} [7-10], and the V_{th} variation also remains the same. Furthermore, SRV is also independent of pulse duration T_{pulse} and amplitude V_{pulse} (**Fig.5a&b**), and only slightly affected by relaxation time T_{relax} (**Fig.5c**). This can be explained by that the longer relaxation process may lead to more localized defects that become inactive at the off-state [5,8], and when the number of remaining active defects become small enough and less uniformly distributed, a slightly larger SRV is observed [8]. *Therefore, the intrinsic stochasticity of the switching in OTS is small and stable, and intrinsic defect clusters leads to consistently small V_{th} variability.*

V_{th} correlated to frequency-domain noise analysis. To further analyze the mechanism of SRV, we developed a fast frequency-domain noise analysis technique, to extract the noise power spectrum density (PSD) of I_{off} and its correlation with V_{th}, SRV and the corresponding defects, at OTS pulse operation conditions. The 1st triangle pulse in the waveform (**Fig. 6a**) is used to switch the OTS on/off to ensure a controllable initial condition. Noise in I_{off} at a certain bias is measured before the end of the 2nd pulse, and V_{th} in the 3rd pulse. Relaxation time T_{relax} and V_{pulse} & T_{pulse} in

the 2nd pulse can be adjusted. Three different regions are observed in the PSD of off-state current noise (Fig.6b). Region 1 is dominated by 1/f noise; Noise in Region 2 begins to increase with bias only when V≥1.6V and is dominated by $1/f^a$ noise where $-0.5 \le a \le -2.5$ (Fig.7a&b); Region 3 is dominated by the noise floor. *OTS noise characteristics in Region 2 are significantly different from those in PCM and other resistive switching devices where only 1/f or $1/f^2$ noise or their combinations can be observed [5,13].*

Clear correlations are observed between PSD of I_{off} in R2 and V_{th} in the 3rd pulse (Fig.8a&b). At a certain bias, a higher PSD leads to a lower V_{th}, due to a larger number of active (delocalized) defects at off-state. Although a higher off-state bias leads to more relaxation during the PSD measurement [12] and the higher V_{th} observed in the next pulse, the variations in PSD and V_{th} are not significantly affected by pulse conditions. It is further supported by the strong correlation between V_{th} and the sum of PSD at a certain bias, where $\sum(S_I)$ = variance (σ^2) (Fig.9a). Relative PSD and variance are less correlated to V_{th} (Figs.8b&9b). This agrees well with the V_{th} and SRV observed in Figs. 4&5. *Therefore, SRV is one of the intrinsic characteristics of OTS switching process, independent of defect cluster sizes and operation conditions.*

IV. LPV characterization and mechanism

Sequential Variability Analysis technique is developed in this work to extract the large V_{th} jumps occurred in cycling shown in Fig.3. V_{th} difference between every two consecutive pulses: $\Delta V_{th,s} = V_{th}^{k} - V_{th}^{k-1}$ is used, in contrast to the conventional V_{th} variation: $\Delta V_{th,o} = V_{th}^{k} - V_{th,\,median}$ [7-9]. $\Delta V_{th,o}$ histograms show typical Gaussian distributions in fresh (single-peak) & degraded (double-peak) OTS devices (Fig.10a), a multimodal CDF in $\Delta V_{th,o}$ can be observed in the degraded OTS (Fig.10b). This is associated with the significantly increased large V_{th} jumps in the degraded device, as $\Delta V_{th,s}$ shows large tails at 1% for both jump-up and jump-down, while the $\Delta V_{th,o}$ distribution becomes multimodal and asymmetric after the degradation. Figs.11a&b demonstrate that V_{th} jumps and recoveries can indeed occur in both directions.

LPV is dependent on on-state operation conditions. In contrast to SRV, larger R_s leads to larger V_{th} jumps, even in fresh devices (Fig.12a). Previous results show that larger R_s leads to a narrower defect cluster [10], hence LPV is more likely to occur in a fresh device with a narrower cluster and it becomes worse in degraded devices (Fig.12b), where the degraded switching energy barriers are lowered [15]. LPV increases with longer T_{pulse} and decreases vice versa, unlike SRV (Fig.13a). Decreasing T_{pulse} again in the same device leads to smaller V_{th} jumps (Fig.13b). This supports the strong correlation between T_{pulse} and V_{th} jumps. *Longer pulses will trigger more and larger V_{th} jumps during the ON-state*.

LPV is independent of off-state operation conditions. On the other hand, V_{th} jumps are not affected by relaxation time T_{relax}, both in fresh (Fig.14a) and degraded devices (Fig.14b). Hence V_{th} jumps are not correlated to the remaining active defects at off-state. V_{th} jumps are not correlated to I_{off} nor OTS sizes either (not shown). Changes of relaxation time T_{relax} by more than 9 orders of magnitude, from the 1 us pulse interval to the inserted 1800 sec relaxation, do not affect or interrupt the gradual V_{th} recovery, as the recovery process resumes from the point before the relaxation (Fig.15a-d). This indicates that the jump/recovery mechanism is different from the defect (de)localization process with different time constants that leads to the V_{th} relaxation [5-8]. Since large V_{th} jumps are strongly correlated with T_{pulse}, albeit less so with V_{pulse}, for both jump-up and jump-down at ON-state (Figs.16a&b), *V_{th} jumps are mainly controlled by ON-state operation conditions.*

Strong correlation with on-state current. A strong correlation between V_{th} and I_{on} is observed (Fig.17), where an increase in I_{on} leads to a reduction in V_{th}, which may be linked to the changes in mobility gap and trap gap [16]. Moreover, details of I_{on} during on-state and its link to V_{th} and V_{hold} is examined. A sudden change of I_{on} leads to a large jump in V_{hold} and then V_{th}, and it can occur in both directions (Fig.18a&b). The amplitude of the ΔI_{on} jump is statistically correlated to the amplitude of ΔV_{th} jump (Fig.19). *This provides strong evidence that LPV is the consequence of DI_{on} jump.*

Multi-modal V_{th} distributions. Complex *V_{th}* distributions have been observed in OTS, and a comprehensive explanation is still missing [7-9]. With the knowledge of SRV and LPV, we can identify the origins of these non-ideal *V_{th}* distributions. A single-modal CDF Gaussian distribution is caused by the SRV alone (Fig.4&5), and a bimodal distribution is caused by one LPV event (Fig.3a&b). When more complex V_{th} behavior occurs, it can be decomposed into multiple LPV and SRV events. For example, different distributions can occur in the same OTS, depending on the operation conditions (Fig.20). Both longer T_{pulse} and larger V_{pulse} lead to more frequent jumps and shorter recoveries, hence different bimodal/multimodal $\Delta V_{th,o}$ distributions.

LPV mechanism and optimization: Amorphous chalcogenides as 'mesoscopic' metastable structures could incur a swift local re-arrangement by stress. Subsequent annealing could then recover these local bonds in a very anisotropic way [17]. Thus, LPV could be the consequence of a local change in OTS material properties occurred at ON-state followed by a slow recovery [6,13] (Fig.21). Similar effect in ReRAM devices was also modelled as the accumulation of small stress leading to a large local change in the filament shape to release the stress [18]. Since LPV is strongly correlated to pulse conditions, a careful selection of shorter T_{pulse} and lower V_{pulse} is essential for reducing LPV, minimizing the OTS degradation and further mitigating the impact of LPV.

V. Conclusions

A detailed investigation on C2C V_{th} variability in GeAsTe OTS devices is carried out in this work. Two different variability mechanisms are identified. SRV is due to the inherent stochastic switching in OTS. LPV consists of a sudden V_{th} jump followed by a slow recovery process and is caused by large I_{on} changes at ON-state, probably due to a large local change in material properties and the following slow recovery. Multimodal V_{th} distributions can be explained by the combination of SRV and LPV under different pulse conditions. A careful selection of operation conditions is needed to reduce LPV and optimize the OTS variability.

References *[1] Z. Zhao, et al, Nano-Mic. Lett. 2024; [2] Y. Koo, et al VLSI 2016; [3] H.Y. Cheng, et al, IEDM 2017; [4] B. Govoreanu, et al, VLSI 2017; [5] Z. Chai et al, VLSI 2019. [6] F. Hatem, IEDM, 2019. [7] D. Garbin, IEDM, 2019; [8] R. Degraeve, IRPS 2021; [9] S Kabuyanagi, et al, VLSI, 2020. [10] Z. Hu, et al TED 2022. [11] T. Ravsher et al IEDM 2021. [12] S.Ban, et al, EDL, 2023. [13] D. Fugazza, et al, IEDM, 2009. [14] J. Lee, et al, IEDM, 2023. [15] M Yamaguchi, et al, IEDM, 2022. [16] S. Clima, et al, ACS Appl. Electron. Mater. 2023. [17] A. Kolobov, et al, physica status solidi (b), 2020. [18] R. Degraeve, et al, IRPS, 2016.*

Acknowledgement: EPSRC of UK (grants: EP/S000259/1 & EP/Y008235/1).

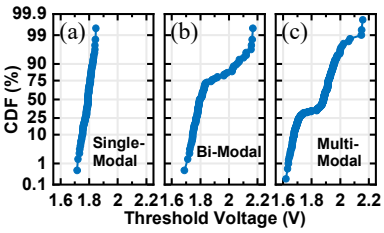

Fig.1 Complex (a) single-, (b) bi- and (c) multi-modal V_{th} CDF can be observed in GeAsTe OTS. Detailed analysis of these CDFs and their operation conditions will be provided in the following sections.

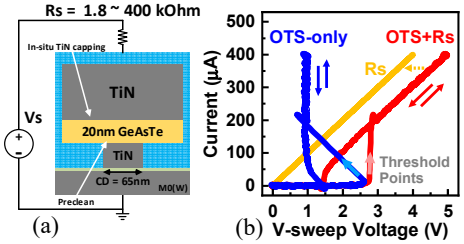

Fig.2 (a) Illustration of the OTS structure in series with an internal resistor R_s. (b) OTS-only I-V (blue) and V_{th_OTS} can be extracted from the I-V of 1S1R_s (red), $V_{th\_OTS}=V_{th,1S1R}-I_{th}\cdot R_s$ (CD: 65nm, Rs: 11kΩ. Pulse edge ramp rate 1V/us is used in this work.)

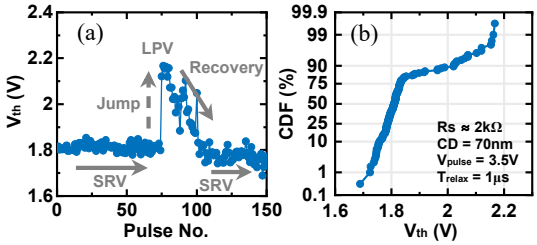

Fig.3 (a) A typical cycle-to-cycle V_{th} variability result consisting of the small random variability (SRV), a large V_{th} jump followed by a gradual recovery process (LPV) measured in 150 cycles, and (b) its bimodal CDF distribution.

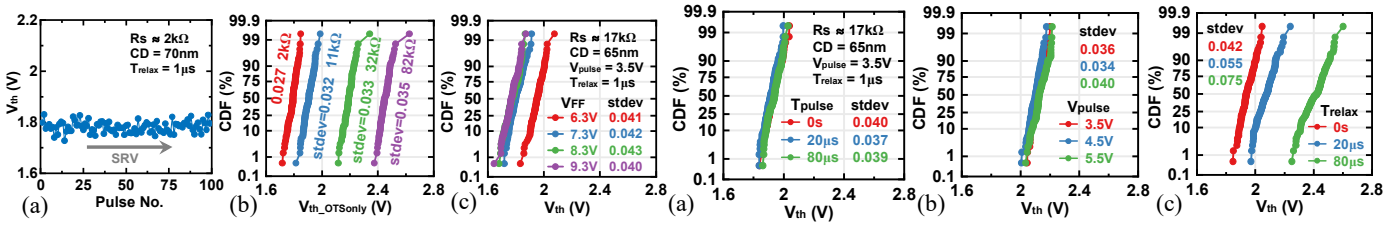

Fig.4 (a) Typical C2C SRV result selected without V_{th} jumps. (b) OTS-only V_{th} increases with R_s, V_{th} variation remains similar, with single-modal Gaussian distributions. (c) Different OTS devices with the same R_s value but different V_{FF}. A larger V_{FF} leads to stronger defect clusters hence a smaller V_{th} and the variation remains same.

Fig.5 SRV is independent of (a) pulse duration T_{pulse} and (b) amplitude V_{pulse}, and (c) is only slightly affected by relaxation time T_{relax}. Longer relaxation process may lead to more localized defects that become inactive, and when the number of remaining active defects become small enough and less uniformly distributed, a slightly larger SRV is observed.

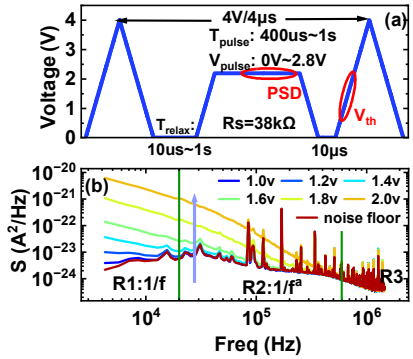

Fig.6 (a) The waveform of fast frequency-domain noise analysis technique to extract the noise power spectrum density in I_{off} under OTS pulse operation conditions. (b) Three different regions are observed in the PSD of off-state current noise.

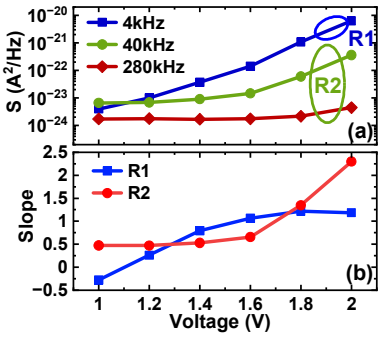

Fig.7 (a) Amplitude and (b) Slope in R1 and R2 in Fig.6. R1 is dominated by 1/f noise; Noise in R2 begins to increase only when V≥1.6V and is dominated by $1/f^a$ noise where $-0.5 \le a \le -2.5$; R3 is dominated by noise floor, which is measured from the probe station and instrument without connecting to OTS.

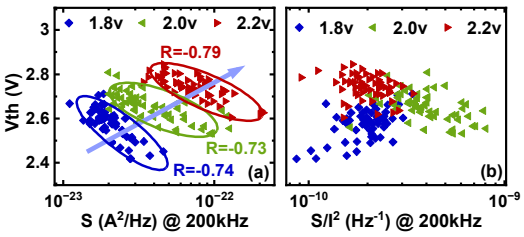

Fig.8 Clear correlations are observed between PSD of I_{off} in R2 and V_{th}. At a certain bias, higher PSD leads to lower V_{th}. Higher off-state bias leads to more relaxation and higher V_{th}. Variations in PSD and V_{th} are not significantly affected by pulse conditions. Correlation coefficient R at each bias is shown and it has similar values at different biases. (b) no clear correlation between relative PSD (S_I/I^2) and V_{th} due to similar contributions by individual defects.

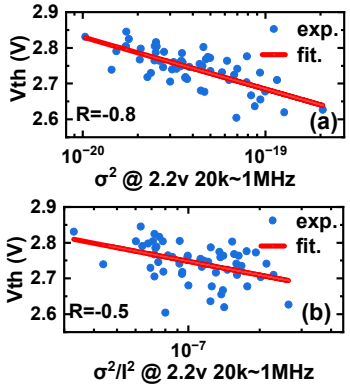

Fig.9 (a) Strong correlation is observed between V_{th} and $\sum(S_I)$ = variance (σ^2) at a certain bias, (b) V_{th} is less correlated with (σ^2/I^2) with a smaller R value, in agreement with V_{th} and SRV observed in Figs. 4&5.

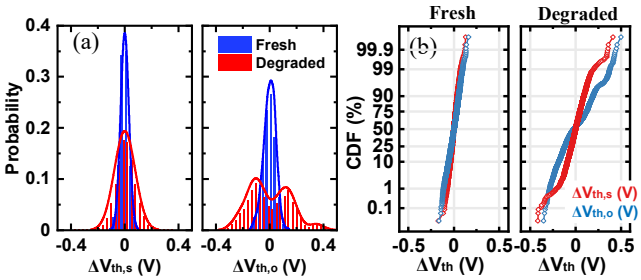

Fig.10 (a) ΔV_{th} histograms shows typical Gaussian distributions in both fresh and degraded OTS devices. (b) Sequential Variability Analysis using the V_{th} difference in every two consecutive pulses, $\Delta V_{th,s} = V_{th}^{k} - V_{th}^{k-1}$, can extract the large V_{th} jumps, which occurred in less than 1% of cycles in both directions. Multimodal and asymmetric CDF in $\Delta V_{th,o}$ can be observed in the degraded OTS due to these large jumps.

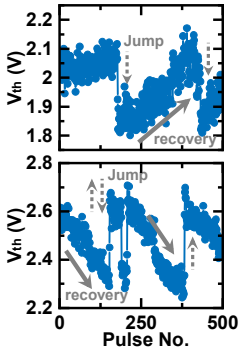

Fig.11 V_{th} jump/recovery can indeed be observed in both directions.

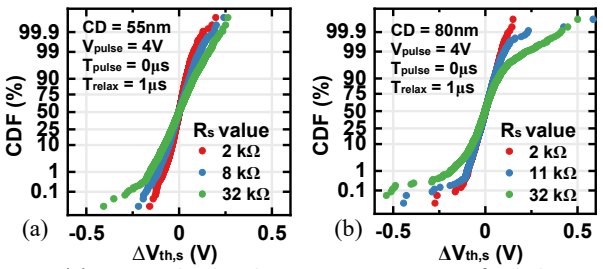

Fig.12 (a) Larger R_s leads to larger V_{th} jumps, even in fresh devices, in contrast to SRV. (b) LPV becomes worse in a degraded device when R_s increases.

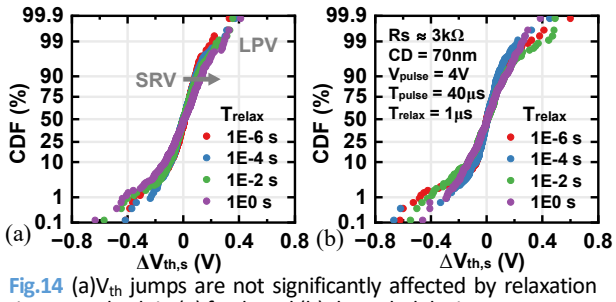

Fig.14 (a)V_{th} jumps are not significantly affected by relaxation time T_{relax}, both in (a) fresh and (b) degraded devices.

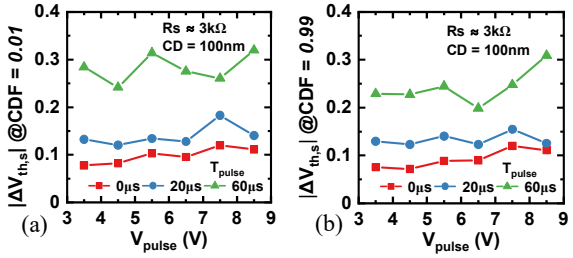

Fig.16 Large V_{th} jump (top 1%) is strongly correlated with T_{pulse}, albeit less so with V_{pulse}, for both (a) jump-up and (b) jump-down.

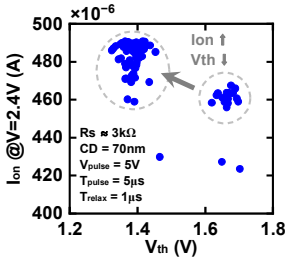

Fig.17 Correlation between I_{on}(@ V_{on}=2.4V) measured in previous triangle pulse and V_{th} of the next triangle pulse is observed.

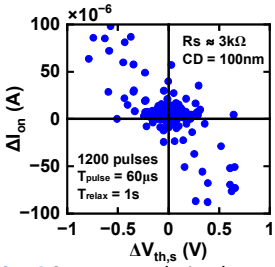

Fig.19 Strong correlation between the amplitudes of DV_{th} jump and DI_{on} jump is observed in ON-state of rectangular pulses in Fig.18.

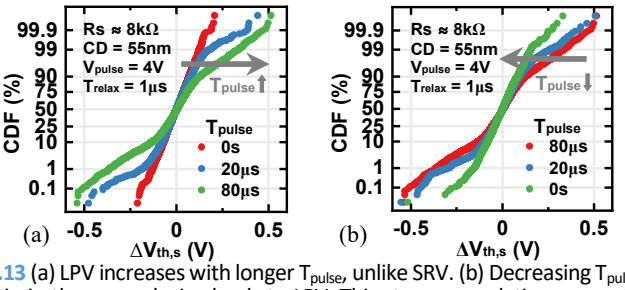

Fig.13 (a) LPV increases with longer T_{pulse}, unlike SRV. (b) Decreasing T_{pulse} again in the same device leads to LPV. This strong correlation supports that these LPVs are mainly caused by T_{pulse}, not by degradation.

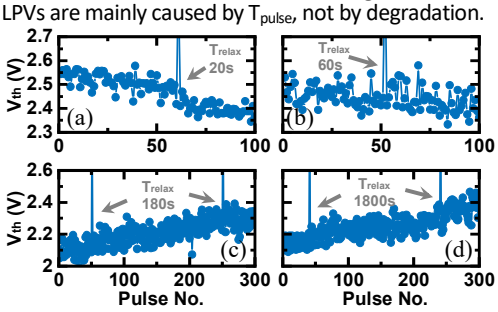

Fig.15 Changes of relaxation time T_{relax} by more than 9 orders of magnitude, from (a) 1 us cycling pulse interval and one 20 sec inserted relaxation, to (d) two 1800 sec inserted relaxation, do not affect or interrupt the gradual V_{th} recovery, as the recovery process resumes from the point before relaxation.

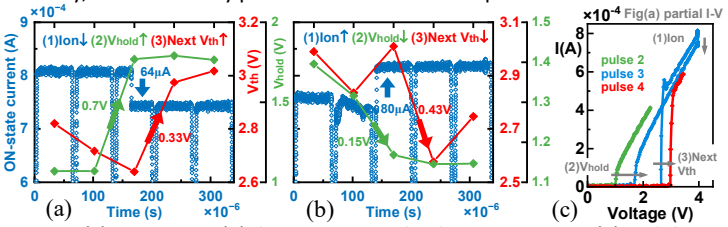

Fig.18 (a) An I_{on} jump (1) during ON-state leads to a V_{hold} jump (2) and then a V_{th} jump in the next pulse (3). (b) Jumps occurred in both directions. (c) I-V measured on the pulse edges in (a), showing ΔI_{on} => ΔV_{hold} => ΔV_{th}.

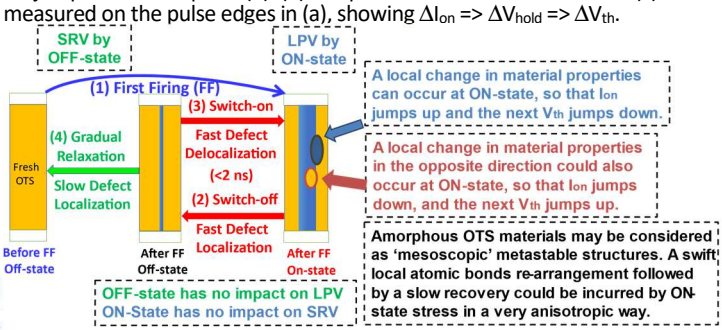

Fig.21 Local changes in material properties could occur at ON-state, causing LPV. SRV is caused by the intrinsic stochasticity of defect clusters in OTS.

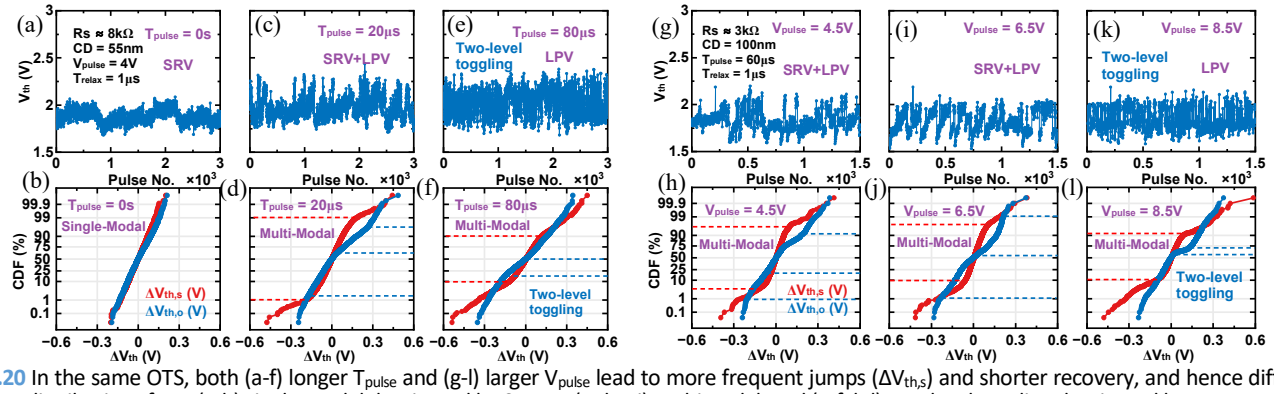

Fig.20 In the same OTS, both (a-f) longer T_{pulse} and (g-l) larger V_{pulse} lead to more frequent jumps ($\Delta V_{th,s}$) and shorter recovery, and hence different $\Delta V_{th,o}$ distributions from (a-b) single-modal dominated by SRV, to (c-d, g-j) multimodal, and (e-f, k-l) two-level toggling dominated by LPV.